Measuring deformation band orientations in the Etchegoin sandstone: Implications for the stress field in central California and the accuracy of emerging orientation measuring technology

Kate Nootenboom
Senior Integrative Exercise
11 March 2020

Submitted in partial fulfillment of the requirements for a Bachelor of Arts degree from Carleton College, Northfield, Minnesota

TABLE OF CONTENTS

Measuring deformation band orientations in the Etchegoin sandstone: Implications for the stress field in central California and the validity of emerging orientation measuring technology

Kate Nootenboom
Senior Integrative Exercise
11 March 2020

Advisor:
Dr. Sarah J. Titus
Department of Geology, Carleton College, Northfield. MN

ABSTRACT

The nuances of stress and strain surrounding the creeping section of the San Andreas fault are poorly understood by structural geologists. Many have conducted studies near Parkfield, California because of its close proximity to the fault trace and unusual seismological history. This study contributes two data sets to the existing data surrounding Parkfield. First, I compare the orientations of planar deformation bands in a 53 m long transect as measured by three separate devices: a Brunton compass, the FieldMove Clino smartphone app, and extraction from a virtual model using CloudCompare's Compass plugin Trace tool. I determine that smartphone measurements are moderately effective when compared against a Brunton, but that virtual extraction is largely unreliable. I then use the Brunton-derived orientations and observed slip amounts to characterize strain using directions of maximum and minimum elongation, from which I infer stress directions including maximum horizontal compression (S_{Hmax}). I find a value for S_{Hmax} of 010°, or 50° from the San Andreas fault strike, and a percent elongation between 2-6%. These findings corroborate previous studies in the same region and support a model of wrench transpression with a mechanically weak zone of distributed shear adjacent to the fault.

Keywords: deformation bands; San Andreas fault; Parkfield, CA; clinometers; stress; strain

INTRODUCTION

This study compares the efficacy of three methods used to measure planar orientations in the field. I compare 292 orientation measurements from the study area taken by a Brunton compass clinometer, a smartphone clinometer app, and digital extraction from a virtual outcrop model created using drone imagery. My findings reinforce the reliability of traditional devices and suggest that new technologies, while promising, require significant advancements before becoming a valid and accessible alternative. The results of this study carry implications both for evaluating the emergent role of technology in the field and for understanding the anomalous stress field surrounding the creeping section of the San Andreas fault.

The San Andreas fault in California remains an enigmatic puzzle for structural geologists, despite being the focus of many decades of research. Motion on the fault is both transcurrent and compressive, and various studies find maximum horizontal compressive stress, or S_{Hmax}, at anomalously high angles to the fault trace that far exceed the expected 30° for a strong fault under Andersonian mechanics (Byerlee, 1987; Mount and Suppe, 1987). The fault is also characterized by a central creeping section where motion is expressed through aseismic creep and micro-seismicity, in contrast to the large magnitude earthquakes that displace the locked segments to the north and south (Scholz et al., 1969; Smith and Wyss, 1968). This zone was initially identified following an unusually high incidence in the early 20th century of earthquakes with ensuing aftershocks and "rapid creep", culminating in the Parkfield, CA earthquake sequence of 1966 (McEvilly et al., 1967; Bakun and Lindh, 1985). The unusual nature of post-seismic stable slip on the fault established Parkfield as a hub for seismologists and structural geologists alike, hoping to uncover answers about the anomalous slip, stress, and strain accommodation along the San Andreas.

Borehole breakout data from the San Andreas Fault Observatory at Depth (SAFOD) suggests an orientation of SHmax between 25° from the fault at the surface to 69° from the fault at depths greater than 2000 m (Zoback and Hickman, 2004; Zoback et al., 2011). Additionally, focal mechanism inversions determine SHmax at 45° from the fault in close proximity to the trace and 50-60° from the fault further afield (Zoback et al., 1987; Provost and Houston, 2001). These orientations differ greatly from those reported by the World Stress Map of 60-85° from the fault (Mount and Suppe, 1987), leading to a debate among geologists surrounding the fault's mechanism of accommodating transpression, for which two models of deformation are proposed (Fig. 1). The wrench transpression model combines the stresses into a distributed shear zone near the fault and is supported by intermediate angles of near-fault S_{Hmax}. The strain- partitioning model decouples the two components into transcurrent motion along the fault and near-perpendicular compression adjacent to the fault (Mount and Suppe, 1987). Recent work suggests that transpression on the fault may have undergone a polyphase evolution from wrench-dominated to strain-partitioned over the last 8 Ma (Bergh et al., 2019).

I infer fault-proximal S_{Hmax} in the Parkfield region from the orientations of deformation bands in the Etchegoin sandstone formation. Deformation bands, and deformed rocks in general, have largely been overlooked as indicators of stress direction in this region and may therefore contain relevant insights to the unresolved debates. I focus on an outcrop of Etchegoin near Parkfield within 2 km of the fault trace (Fig. 2). I use orientation data for 275 deformation bands measured along a 53 m transect, along with apparent slip amounts, to calculate strain percentages and principal axes under two end-member conditions: assumed normal, dip-slip displacement, and assumed strike-slip displacement. I then use the axis of minimum elongation to approximate the regional orientation of S_{Hmax} acting on the outcrop based on physical deformation of rocks in Parkfield, and use these findings as an important check on previous orientations inferred from focal mechanism and borehole breakout data.

GEOLOGIC BACKGROUND

I focus on deformation bands in the Etchegoin Formation, a marine sandstone deposited in the San Joaquin basin during the late Miocene and early Pliocene (Loomis, 1990). Stratigraphically, it overlies the Monterey Formation and underlies the San Joaquin Formation, and records the overall regression of the San Joaquin sea as caused by increased sedimentation rates from uplift of the Temblor and Diablo ranges (Loomis, 1990). The Etchegoin Formation is described as a coarse-grained, poorly indurated, detrital sandstone with high porosity, between 30-40%, and therefore high permeability (Link et al., 1986; Loomis, 1990; Sheirer and Magoon, 2007; Lindquist, 2018). Post- depositional deformation of the Etchegoin Formation is expressed near Parkfield as folding known as the Parkfield Syncline (Dickinson, 1966). Folding is thought to have initiated in the region as early as the Eocene, with extensive refolding occurring in the Pleistocene (Harding, 1976; Wentworth and Zoback, 1989).

In addition to these map-scale processes, deformation in the Etchegoin Formation is expressed on the grain-scale by the creation of deformation bands. Deformation bands are strain localization planes that form in porous, granular material. They evolve as a result of grain reorganization from cataclasis, rotation, or translation, and are classified along a spectrum of pure compaction to pure dilation with a midpoint of simple shear (Fig. 3; Schultz and Siddhartan, 2005; Fossen et al., 2007). Most deformation bands have some component of shear to accompany either compaction or dilation and can accommodate mm- to cm- scale displacement (Schultz and Siddhartan, 2005). Field observations in the study area suggest that an individual deformation band accommodates, on average, 1 cm of slip.

Deformation bands in the Etchegoin sandstone are thought to be a result of both compaction and simple shear (Lindquist, 2018). The high porosity of the sandstone makes it particularly susceptible to compaction band localization, and the resulting bands are characterized by a notable reduction in both porosity and permeability from cataclasis (Lindquist, 2018). Cluster zones of multiple deformation bands are also common in the Etchegoin and are considered a result of the limited ability of an individual deformation band to accommodate slip. Individual bands typically do not exceed a centimeter in width, but cluster zones can exist on the decimeter to meter scale.

It is important to note that deformation bands themselves are not slip surfaces, but that slip surfaces can and often do form within bands or zones of bands and can eventually lead to high-offset faulting at later stages of development (Fossen et al., 2017). Field observations suggest that the width of a cluster roughly equals, in centimeters, the number of deformation bands in that cluster (Fig. 4), and that displacement along zones follows the same generalized ratio for displacement along individual bands: for every band in a cluster, offset increases by 1 cm (Newman, 2011). Deformation bands in the study transect can therefore be viewed as “proto-faults” in porous sandstones and assigned an amount of slip following the 1:1 cm ratio.

TASK 1: DEVICE COMPARISON

Structural geologists have traditionally relied upon analog compasses, such as Bruntons, Freibergs, or Silvas, to measure orientations in the field (Allmendinger et al., 2017). However, emerging technologies now hold the potential to greatly increase the efficiency of orientation measurements taken. Dominant among these are smartphone compass apps and virtual outcrop models, which are reconstructed from images using Structure from Motion (SfM) photogrammetry technology (Allmendinger et al., 2017; Cawood et al., 2017; Novakova and Pavlis, 2017). While some researchers have had relative success with smartphone compasses and virtual models (Allmendinger et al., 2017; Cawood et al., 2017), recent work has revealed a concerning lack of stability in smartphone magnetic sensors, particularly in Android devices (Novakova and Pavlis, 2017). Prior to this study, no comprehensive comparison existed between all three methods.

In this paper, I compare three representative devices from each category: a Brunton as a traditional analog compass, the FieldMove Clino App on an Apple iPhone 7, and a virtual model reconstructed from images taken by a Phantom 4 Pro (DJI) Unmanned Aerial Vehicle (UAV). I assume that Brunton clinometers yield the most accurate measurements based on many decades of dependable implementation in the field.

METHODS

In December 2019, Sarah Titus, Chelsea Scott, Nora Mertz and I collected measurements along a 53 m transect at an outcrop of Etchegoin sandstone near Parkfield, CA. We measured the orientations of 303 deformation bands or deformation band clusters using a traditional Brunton compass clinometer followed by the FieldMove Clino App on an Apple iPhone 7. We also collected images of the outcrop using a UAV, which I later used to construct a virtual outcrop model in AgiSoft Photoscan Pro (v.1.4.5) using Structure-from-Motion technology (Fig. 6; Tavani et al., 2013; Cawood et al., 2017). I then use the software CloudCompare and its internal Compass plugin Trace tool to extract orientation measurements from the virtual model for 292 of the original 303 planes (Fig. 7). I deemed 11 not viable due to low resolution. The orientations of these 292 planes were measured independently by each device, and therefore form the sample population of the statistical comparison.

I chose to compare the measurements between devices using an angular mismatch approach, following the analysis performed by Allmendinger et al (2017), in order to minimize bias introduced by the varying measurement mechanisms. Compass clinometers, like the Brunton, report orientations in two measurements: a strike azimuth and a dip angle down from horizontal. These measurements are taken separately and require interim movement of the compass. Smartphone apps, like FieldMove Clino, also report a dip angle but give a dip direction azimuth instead of a strike, and both measurements are taken synchronously without movement of the device (Allmendinger et al., 2017). Digital plane extraction, as performed using CloudCompare, returns a strike and dip simultaneously based on alignment of points in a 3D point cloud (Dewez et al., 2016).

The variations in technique between the devices renders a simple side-by-side comparison, such as strike vs. strike or dip vs. dip, incomprehensive (Allmendinger et al., 2017). Instead, I use the program Stereonet to compute the mismatch angle, or angle between poles-to-planes, and thus can compare the orientations with a single numerical value. A low mismatch angle indicates good agreement between devices, and a high mismatch angle indicates poor agreement. Allmendinger et al (2017) establishes 4° as a standard maximum mismatch angle to be expected between multiple measurements of the same plane by an analog compass, attributed to human error.

RESULTS

The greatest agreement existed between measurements reported for a single deformation band by the Brunton and the FieldMove Clino app, with a mean mismatch angle of 13.1° and a standard deviation of 9.9. This is in contrast to the mean mismatch of 34.8° (sd = 24.9) between the Brunton and the virtual model, and the mean mismatch of 34.9° (sd = 25.7) between the app and the virtual model (Table 1; Fig. 8). These findings suggest that the FieldMove Clino app performs moderately well in comparison to the standard Brunton compass, but that extraction from a virtual model rarely returns reliable measurements (Fig. 9). The remarkable similarity in the disagreement between the virtual model and both the Brunton and the FieldMove Clino app suggests that agreement with the virtual extraction technique was not preferentially skewed towards either.

I sorted the mismatch angles between the Brunton compass and virtual extraction technique into three categories and plotted each on separate stereonets based on level of agreement: good (0-30°), moderate (31-60°), and poor (61-90°). These plots reveal that no strong pattern exists of a consistent Brunton-derived orientation that is most poorly measured by the virtual extraction. In other words, all orientations are susceptible to mismeasurement by the virtual extraction technique. However, the poorly matched orientations extracted from the virtual outcrop consistently fall in the upper right (NE) quadrant and suggest that the extraction technique is preferentially biased towards reporting planes that dip with moderate to high steepness towards the SW, regardless of the true orientation of the plane (Fig. 9).

TASK 2: STRAIN ANALYSIS

All measurements used for strain analysis were taken by a Brunton compass clinometer. I used 275 orientation measurements from the transect for calculations. See Figure 10 for explanatory schematics of calculations.

METHODS

Field observations primarily indicate normal or strike-slip motion along slip surfaces. However, the two motions are often indistinguishable in the field , and true displacement amounts can be difficult to observe (Fig. 5). I therefore calculate percent strain under two assumed end-member scenarios: 1) all deformation bands in the transect are behaving as normal faults, 2) all deformation bands in the transect are behaving as strike-slip faults. Additionally, field observations suggest that most deformation bands in the Etchegoin fall into one of three general orientation trends: a right-lateral group striking 280° with a shallow dip to the north, a right-lateral group striking 350° with a steep dip to the east, and a left-lateral group striking 220° with a steep dip to the northwest. Therefore, I assign sense of motion to each band under assumed strike-slip conditions according to strike.

Assumed Normal Motion

I first calculated the true horizontal change in length (ΔL_t) in the dip direction for each deformation band or band cluster, assuming 1 cm of dip-slip motion, using the following formula:

$$\Delta L_t = n \bullet \cos\theta$$

where n = number of deformation bands in a cluster (n = 1 if not a cluster) and θ = the dip of the deformation band or cluster. I then used ΔL_t to compute the apparent change in length (ΔL_a) that would be observed on a hypothetical, projected transect with a vertical face and an assigned strike, using the following formula:

$$\Delta L_a = \Delta L_t \bullet \cos\alpha$$

where α = the difference between the dip direction of the deformation band and the strike of the projected transect. I performed this operation for every deformation band or cluster and summed the results to find the total apparent change in length (ΔL_{atot}) along a projected transect. I found ΔL_{atot} for projected transects between 0-180° inclusively, at intervals of 10°. The strike of the projected transect with the highest ΔL_{atot} gives the approximate direction of maximum elongation.

Assumed Strike-Slip Motion

For assumed pure strike-slip motion, the true horizontal change in length (ΔL_t) is simply the number of deformations bands in a cluster multiplied by 1 cm. The apparent change in length on a projected transect, therefore, is

$$\Delta L_a = \Delta L_t \cdot \cos\delta$$

where δ = the difference between the strike of the deformation band and the strike of the projected transect. Depending on the value of δ and the sense of motion of the deformation band, this change in length may manifest as either elongation (ΔL_a) or shortening ($-\Delta L_a$). I assigned sense of motion to each deformation band based on an established pattern observed in the field: bands striking between 015° and 100° were assigned left-lateral motion, and bands striking within 000°-015° and 100°-180° were assigned right-lateral motion. I refer the reader to Appendix A for complete rules and an example calculation. Following the strategy used under assumed normal conditions, I calculated ΔL_{atot} for projected transects between 0-180° inclusively, at intervals of 10°, with the strike of the projected transect with the highest ΔL_{atot} interpreted as the approximate direction of maximum elongation.

RESULTS

Under assumed normal motion conditions, I found a maximum L_{atot} of 116 cm at 100° and a minimum L_{atot} of 68 cm at 170°. Under assumed pure strike-slip conditions, I found a maximum L_{atot} of 329 cm at 100°, and a minimum L_{atot} of -562 cm at 010°. Together, these findings indicate a maximum elongation direction (S1) at azimuth 100°, and a range of minimum elongation direction (S3), or shortening in the case of pure strike-slip, between 350-010° (Fig. 11). Because principal strain axes are, by definition, orthogonal, this study assumes 010° as the best approximation of regional shortening.

Conveniently, the direction of maximum elongation is almost parallel to the true strike of the outcrop face at the study area, which varied along the transect but averaged to about 110°. Therefore, I was able to roughly calculate the percent elongation under both pure strike-slip and pure normal assumed motion using the following formula:

$$e = \Delta L / L_i$$

where ΔL is equal to the maximum positive change in length and L_i is equal to the initial length of the deformed area, which I calculated by subtracting the change in length from the measured final length of 53 m. I found 2% elongation assuming normal motion and 6% elongation assuming strike-slip motion.

DISCUSSION

Device Comparison

The comparison of three orientation measurements devices reinforces the reliability of traditional compass clinometers and reveals promising applications for smartphone apps used on Apple iPhones. However, the 13.1° mean mismatch angle between the Brunton compass and the FieldMove Clino app is much higher than the established 4° mismatch angle of error for the Brunton compass alone, and therefore the app is not yet viable as a perfect substitute for analog compasses. The high angles of mismatch between the virtual outcrop extraction method and both the app and analog methods indicate that virtual extraction is far from universally reliable and requires significant advancements before full implementation in the field. The extraction consistently reported false orientations of planes dipping moderately to steeply towards the SW, suggesting that this technology is not only unreliable in its measuring capabilities, but is also preferentially biased to report an orientation that does not exist in the field.

Previous studies have found virtual outcrop models to be reliable reporters of structure orientation (Tavani et al., 2016; Vasuki et al., 2014). The success of these studies likely relies upon access to high-power data processing machines, which allow for greater image resolution and semi-automatic analysis of abundant data. Though virtual outcrop models may one day be suitable, and even preferable, for rapid processing of large-scale and hard-to-reach study areas, I find that significant barriers still do exist that render such technology unreliable and largely inaccessible at the undergraduate level, especially in contrast to the readily available analog compasses and near ubiquity of smartphones.

Strain Analysis

This study provides necessary corroborative evidence for an intermediate S_{Hmax} in close proximity to the creeping section of the San Andreas fault. Using the azimuths of the maximum and minimum principal strain axes determined from the Parkfield transect, I infer a regional S_{Hmax} value equivalent to the minimum elongation direction at 010°. This is oblique to the San Andreas fault at an angle of 50°, which is considerably more intermediate than the S_{Hmax} values of 60-85° reported by the World Stress Map (Mount and Suppe, 1987) but is still too high to explain transcurrent motion under Andersonian mechanics (Byerlee, 1978; Scholz, 2000).

Other work in the creeping section of the San Andreas fault corroborates an intermediate angle of S_{Hmax}. Notably, Provost and Houston (2001) use focal mechanism data from the Parkfield region to find an orientation for S_{Hmax} at ~45° from the fault in a 1-3 km wide zone of mechanical weakness. Focal mechanisms from the southern section of the fault also show intermediate S_{Hmax} values of 40-50° in a 5-50 km wide zone (Hardebeck and Hauksson, 1999). The use of focal mechanism data, however, has been shown to be susceptible to misinterpretation even when the data yield consistent results (Hardebeck and Michael, 2004). My results therefore provide a necessary check on previous constraints of S_{hmax} orientations.

An intermediate angle of S_{Hmax} supports the wrench-dominated transpression model of strain accommodation, which relies upon a region of distributed simple shear adjacent to the fault (Fig. 12; Mount and Suppe, 1987; Fossen et al., 1994). The proximity of the study area to the San Andreas, coupled with the intermediate obliquity of the strain axes, indicates distributed shear occurs in a zone at least 2 km from the fault trace and disqualifies a model of pure stain-partitioning in the region. This study confirms previous studies that find distributed shear in a narrow, near-fault, mechanically weak zone near Parkfield, and establishes deformation bands as appropriate indicators of principle strain axes when analyzed as slip surfaces.

Future research

Future work with deformation bands in the Parkfield area or comparisons between orientation measurement devices can improve upon the limitations of this study in several ways. These include:

- Exploration of alternative comparison methods between devices. I deemed a mismatch angle approach most appropriate to compare orientations based on the varying mechanics of each device. However, this technique does not indicate which element is most problematic between two disagreeing measurements. For example, measurements may be similar in strike but vastly different in dip, or vice versa, but this specificity is not available using a mismatch angle approach.
- Address impact of volume change on strain. I assume negligible change of outcrop volume during deformation. However, the creation of deformation bands inherently implies a change in grain size and porosity, which would impact measurements of transect length used to calculate percent strain. Therefore, the percent elongations found in this study represent maximum values.

- Strain analysis with respect to deformation chronology. Recent work has suggested that strain accommodation on the San Andreas has undergone a polyphase evolution from wrench-dominated to strain-partitioned over the last 8 Ma (Bergh et al., 2019). Field observations of cross-cutting relationships suggest that groups of similar-oriented deformation bands may have formed concurrently at different time intervals, and may therefore record variations in the stress field. I treat all deformation bands as equal indicators of a single stress direction in this study. However, future studies may wish to perform strain analyses on groups of concurrently formed deformation bands to identify a pattern of evolution.

CONCLUSION

“I disbelieve, and therefore strongly resent, the notion that I or anybody else could write better or more easily with a computer than with a pencil.”

~Wendell Berry

Emerging orientation measurement devices, such as the FieldMove Clino smartphone app and virtual extraction from UAV imagery, are not yet viable as substitutes for traditional compass clinometers. Smartphone apps perform moderately well against a Brunton compass, but virtual extraction techniques require significant advancements before reliable implementation. These findings suggest that physical presence in the field is still an integral and irreplaceable aspect of geology.

Deformation bands in the Etchegoin sandstone near Parkfield, CA, can be used as strain indicators to constrain maximum horizontal compressive stress. A strain analysis performed on an outcrop of deformed Etchegoin found between 2-6% elongation along the direction of maximum elongation (100°), and oriented S_{Hmax} at 010°, or 50° from the San Andreas fault trace. This intermediate value aligns with orientations of S_{Hmax} from previous studies in the same region derived from borehole breakout analysis and focal mechanism inversion, indicating a narrow, mechanically weak zone of distributed shear adjacent to the fault.

ACKNOWLEDGEMENTS

I thank my professors and classmates in the Carleton Geology Department for their guidance, support, and general camaraderie over the past three years. Additionally, I am grateful to Chelsea Scott, Nora Mertz, and Lena Nyblade for their assistance in the field with data collection; this project would not have been possible without them. I'd like to thank my advisor, Sarah Titus, for providing invaluable experiences in the field, lab, and classroom. Finally, a big thank you to my friends and family for their love, support and late-night phone calls throughout this process. Funding for this project was provided by the Petroleum Research Fund.

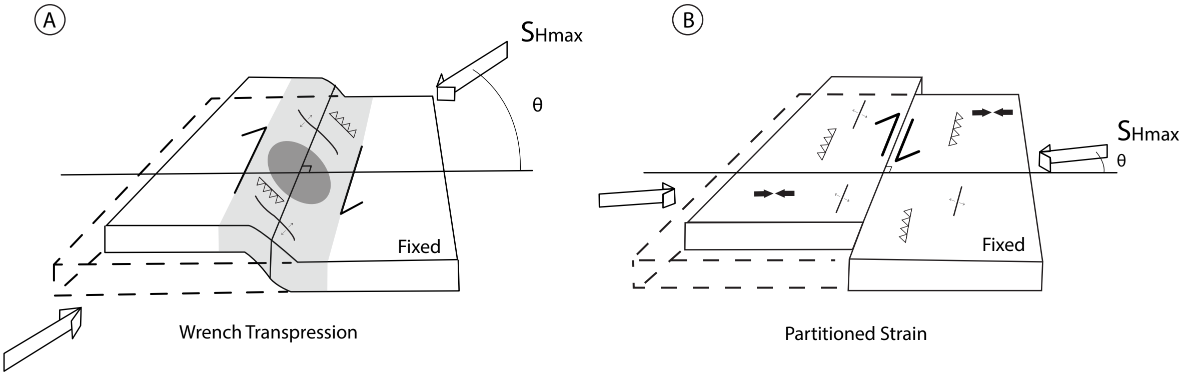

Figure 1. A) Model of wrench deformation along a strike-slip fault. S_{Hmax} is oriented at an intermediate angle to the fault. Gray shading represents a region of distributed shear adjacent to the fault, with fold, fault, and strain ellipse axes shown perpendicular to S_{Hmax}. B) Model of partitioned strain along a strike-slip fault. Transcurrent motion is accommodated by strike-slip along the fault plane, and compression is accommo-dated off-fault through faulting and folding. S_{Hmax} is oriented at a near-perpendicular angle to the fault. Figure adapted from Mount and Suppe, 1987.

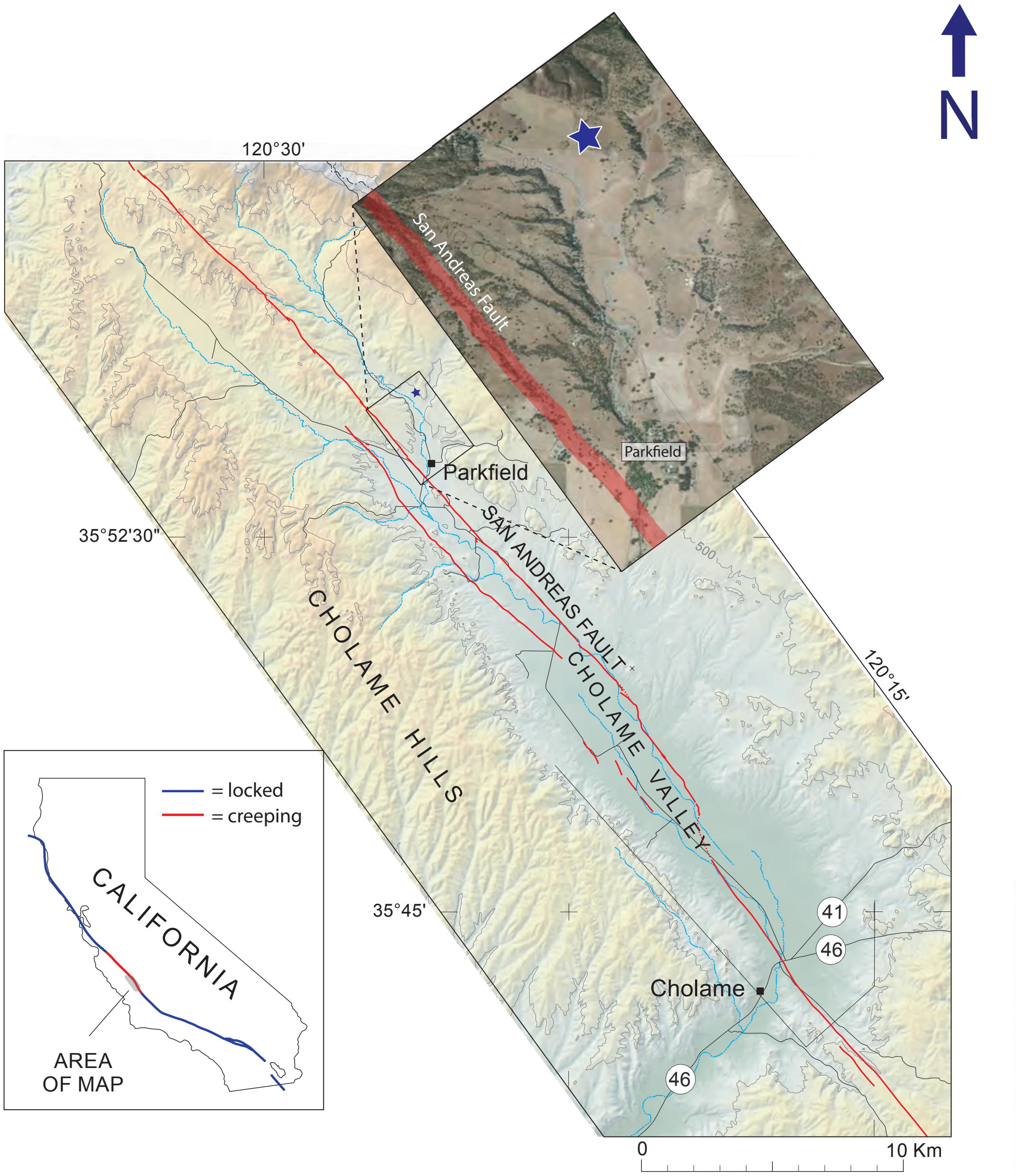

Figure 2. Map of Parkfield area in central California. Blue star shows location of study area and proximity to Parkfield and the San Andreas fault. Inset of California outline shows creeping and locked segments of the fault. Figure adapted from Zoback et al, 2011.

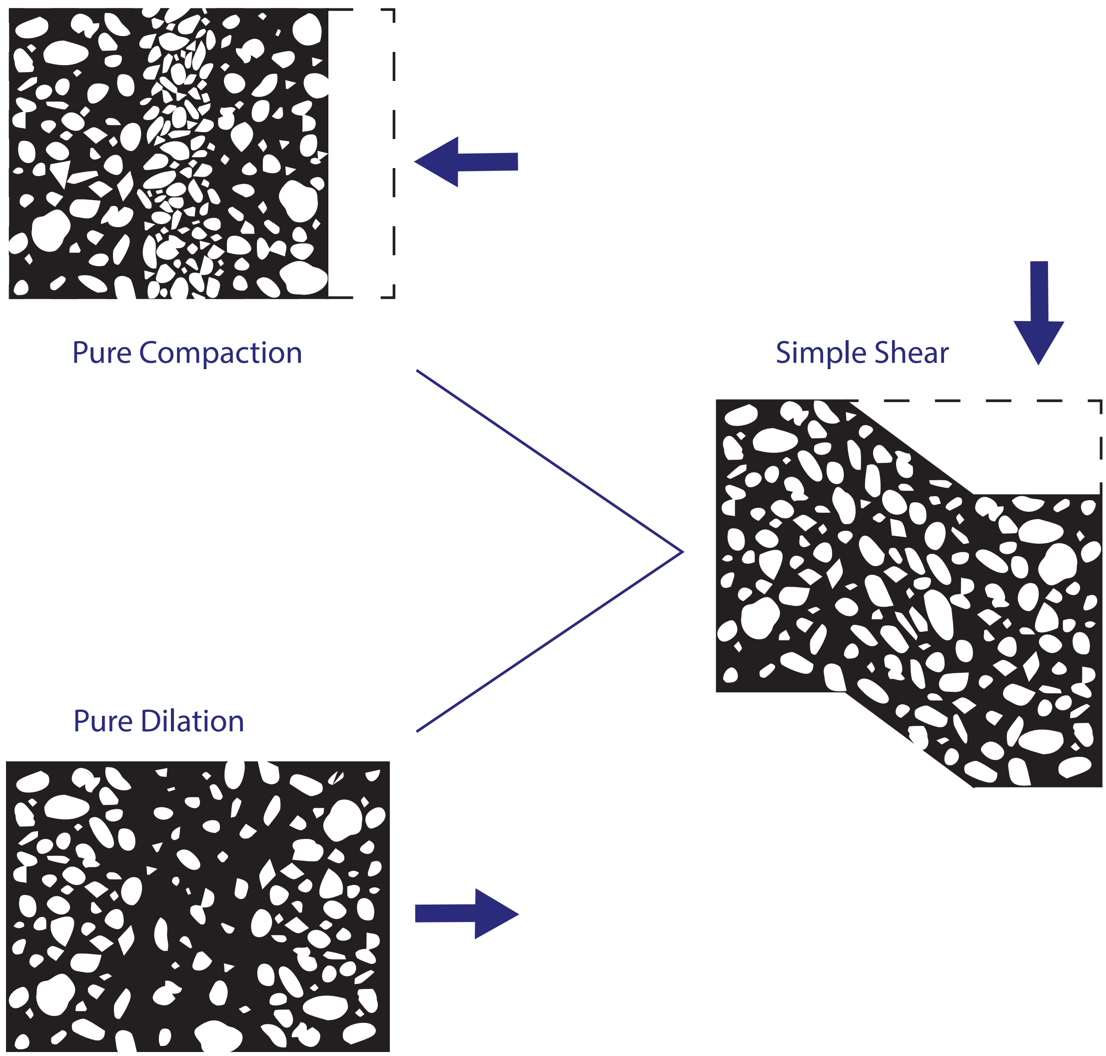

Figure 3. Schematic depicting grain-scale processes behind the three main types of deformation bands: pure compaction, simple shear, and pure dilation. Many deformation bands exist as either compaction or dilation bands, with a component of shear. Figure adapted from Fossen et al, 2007

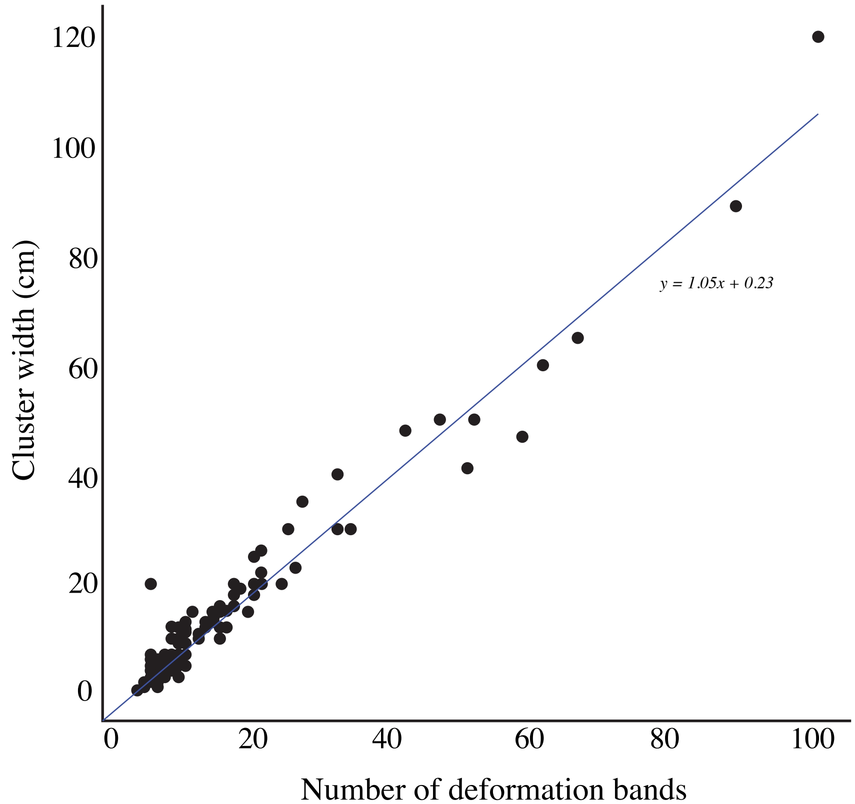

Figure 4. Plot showing 1:1 ratio of deformation band count to cluster width.

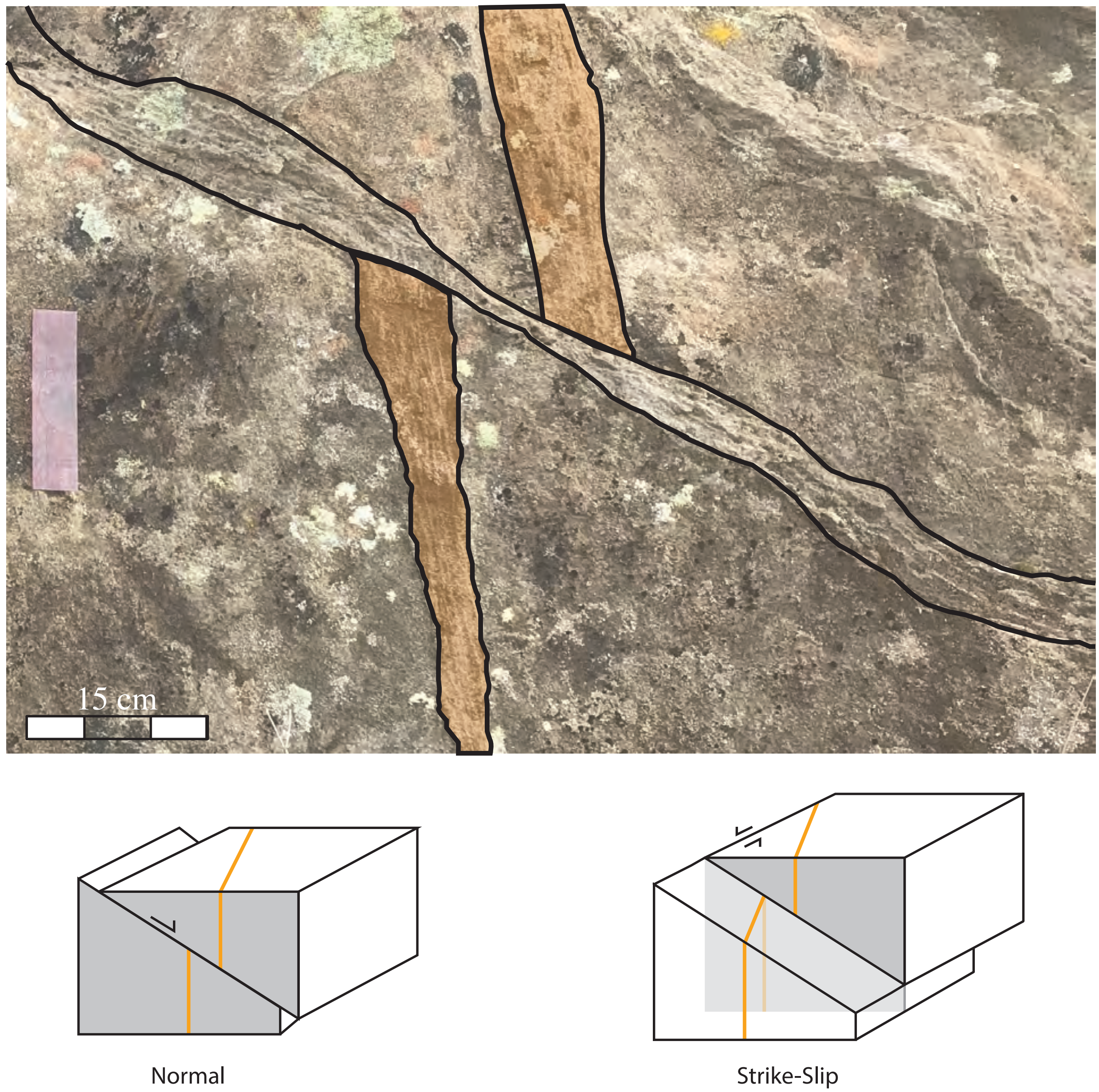

Figure 5. Example field photo of displacement along a deformation band cluster. Block diagrams show two possible senses of motion to explain apparent offset: normal slip (left) and strike-slip (right).

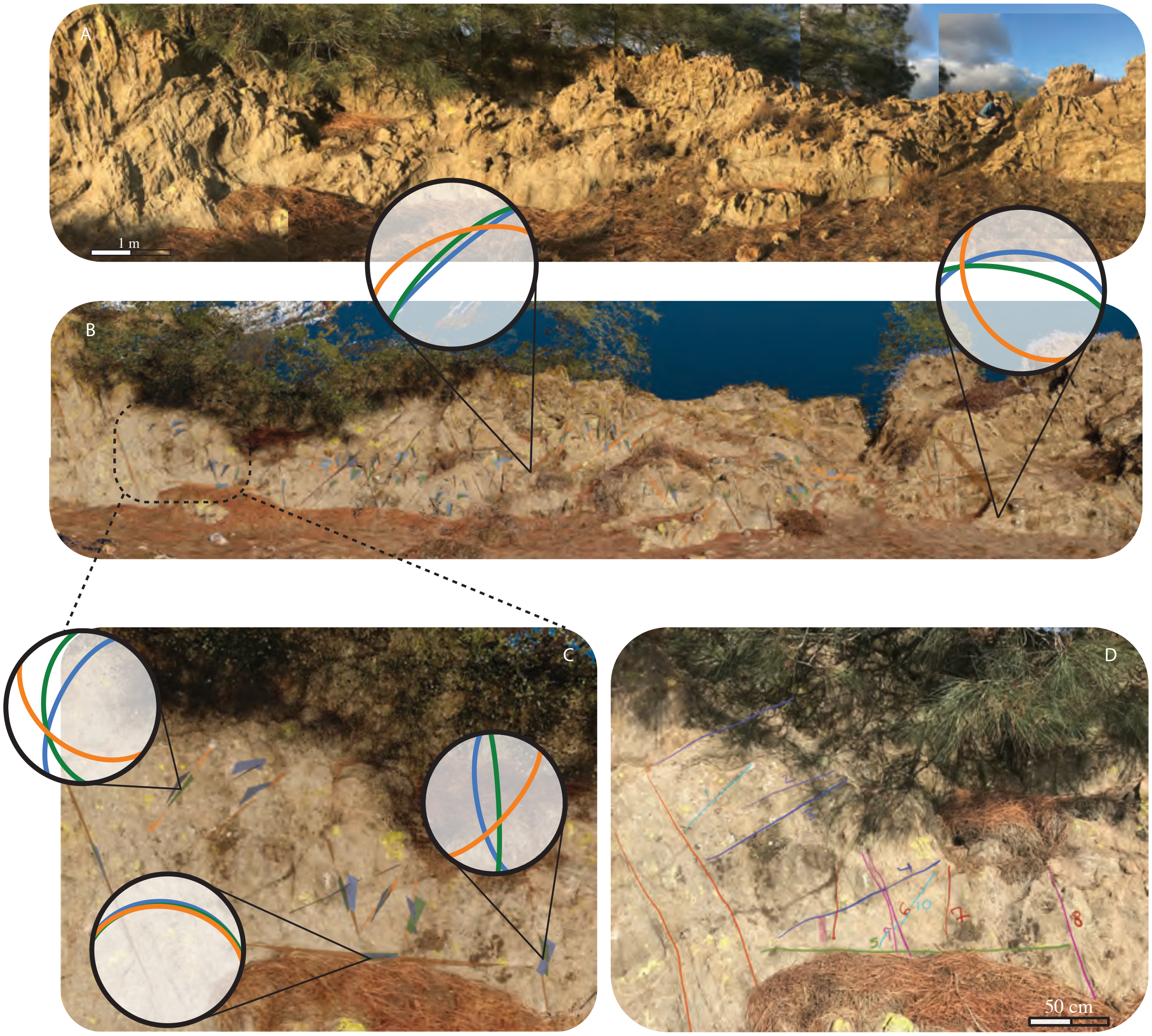

Figure 6. The first section of the study transect as landscape photo panorama (A) and virtual outcrop model (B). A sample zoom-in section of the virtual outcrop (C) with corresponding annotated photograph of transect section with selected deformation bands for orientation measurement. Stereonets show orientations of deformation bands as measured by: Brunton compass (blue), FieldMove Clino app (green), and digital extraction from the virtual outcrop (orange).

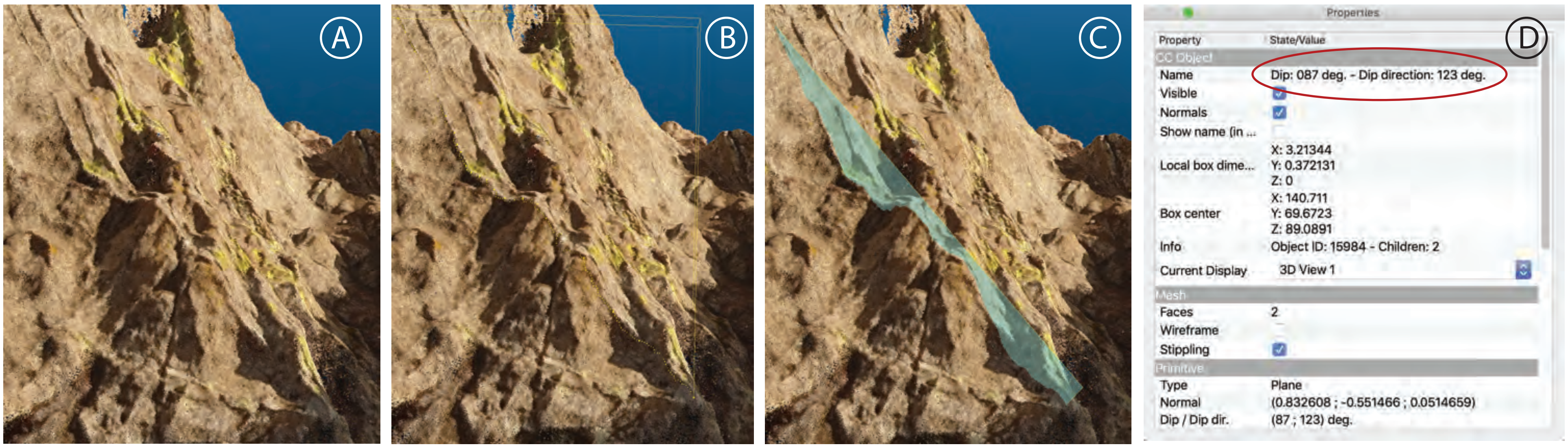

Figure 7. Example sequence of plane orientation extraction from a virtual outcrop model. Panels A-C show the process of plane identification and fitting in CloudCompare using the Compass plugin's Trace tool, panel D shows example output of orientation data.

page left intentionally blank for formatting purposes

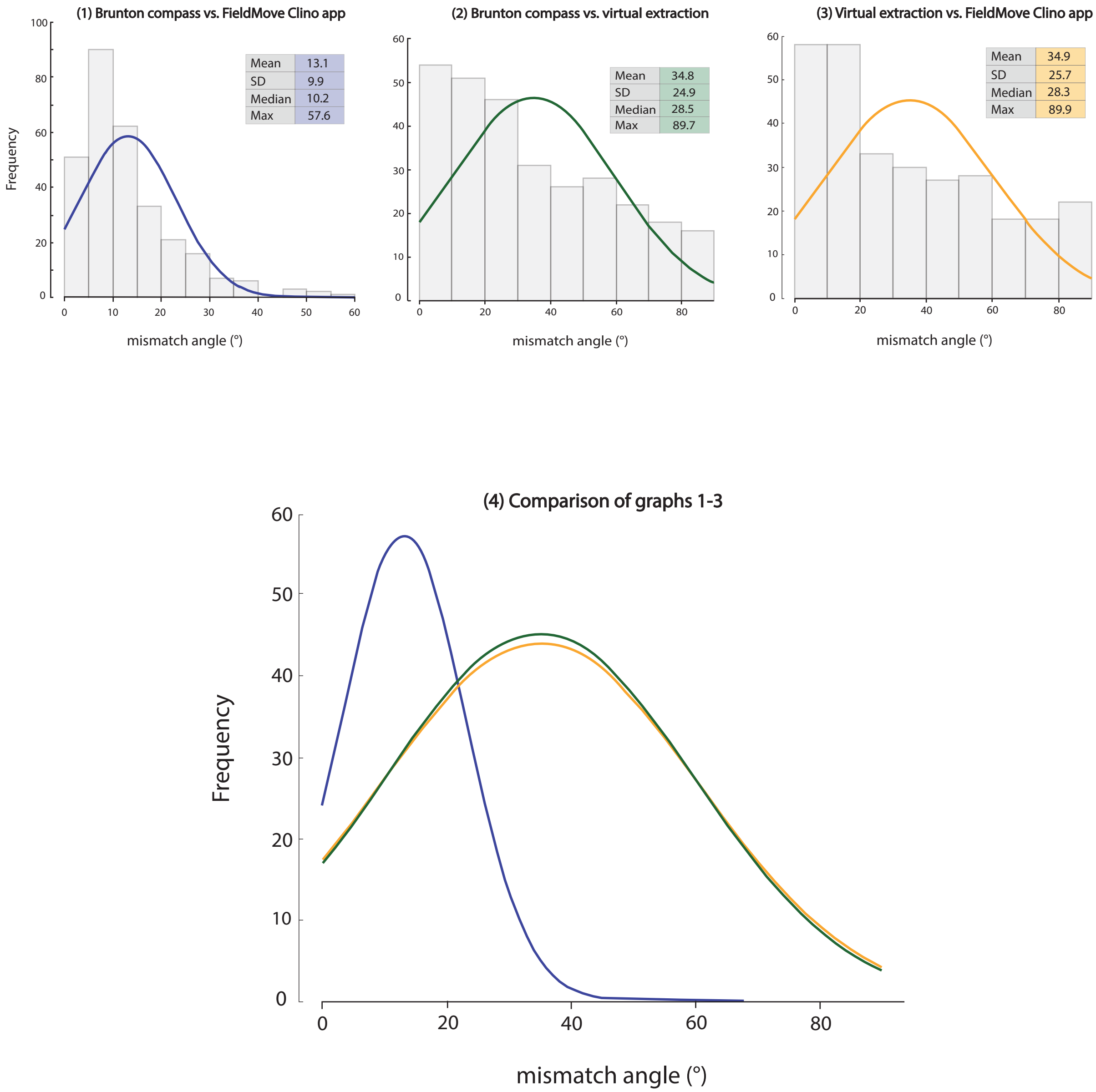

Figure 8. Frequency distributions of mismatch angles between Brunton compass and FieldMove Clino app (1), Brunton compass and virtual extraction (2), and virtual extraction and FieldMove Clino app (3). Distribution curves for each comparison are plotted together for direct juxtaposition (4).

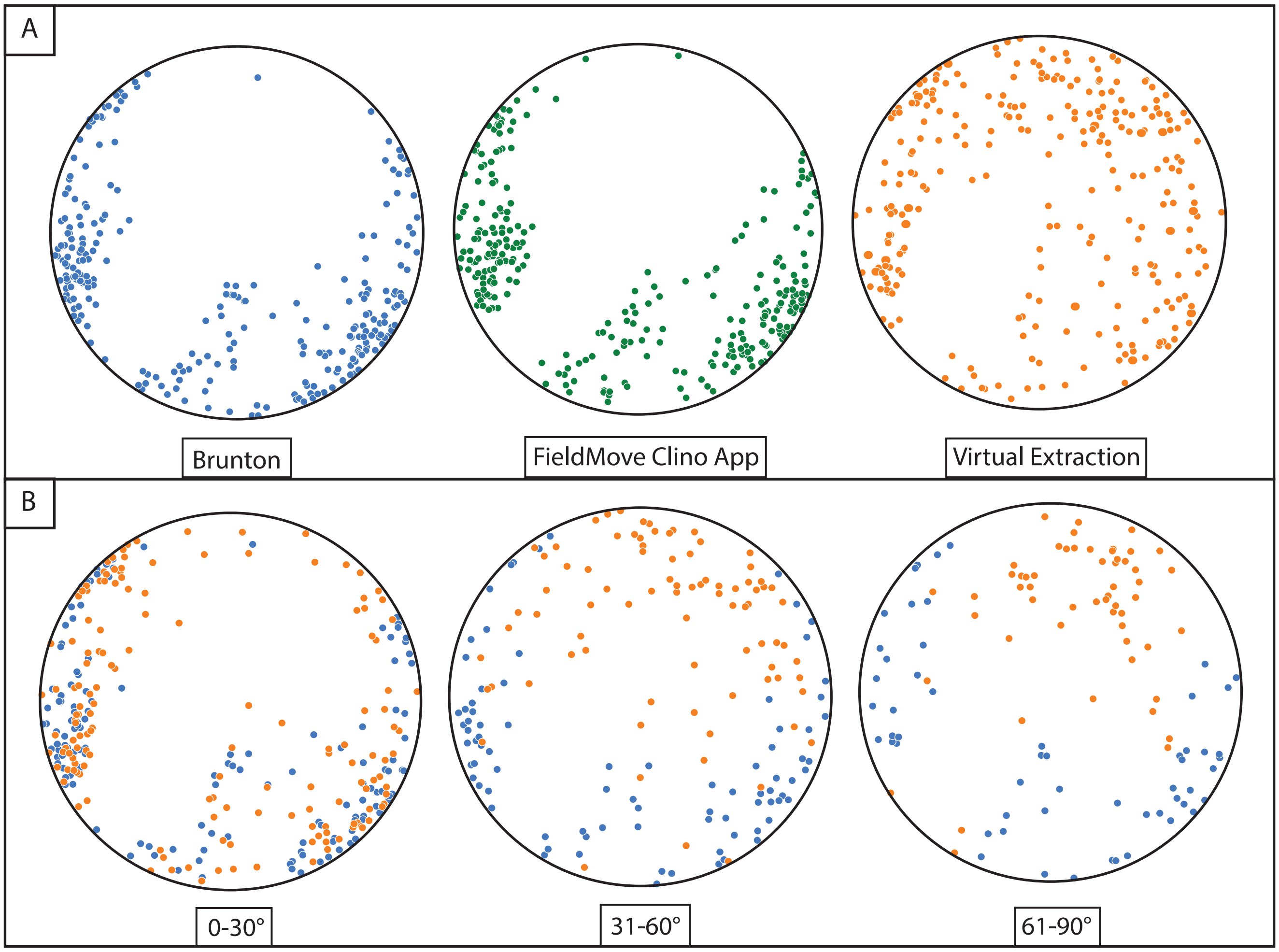

Figure 9. A) Stereonets showing poles to planes for deformation bands measured by Brunton compass (left, blue), FieldMove Clino app (middle, green), and extraction from a virtual model (orange, right). Good agreement is apparent between Brunton and FieldMove Clino measurements. Virtually extracted measurements are in noticeably poor agreement with the other two devices. B) Stereonets showing poles to planes for deformation bands measured by Brunton compass (blue) and extraction from virtual outcrop (orange). From left to right, stereonets show good agreement (<30° mismatch), moderate agreement (31-60° mismatch), and poor agreement (61-90° mismatch). There does not appear to be a consistent Brunton-derived orientation that is poorly measured by the virtual model; however, the poorly measured orientations from the virtual model are consistently scattered in the upper right (NE) quadrant of the stereonet.

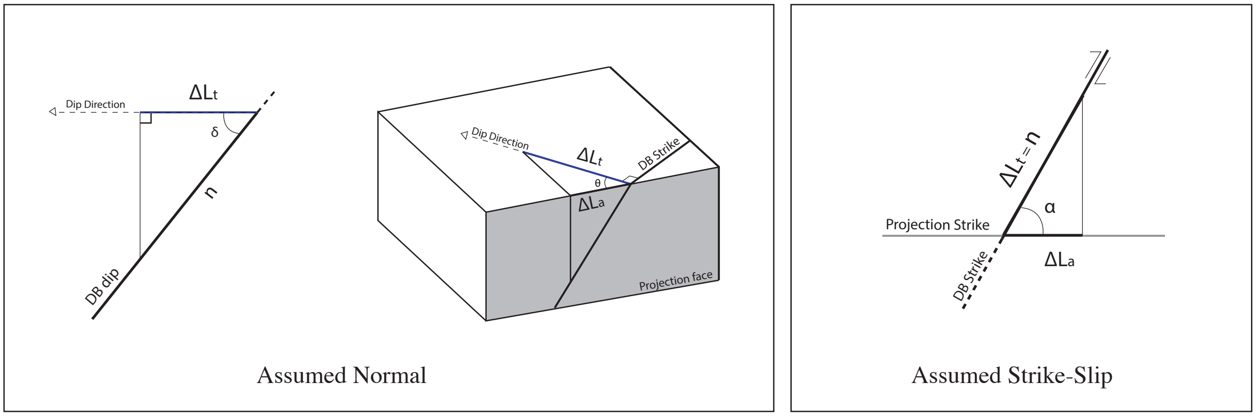

Figure 10. Schematic diagrams illustrating calculations for ΔLt and ΔLa under assumed normal (a) and strike-slip (b) conditions. Assumed normal calculations are shown in cross-section view (left) and block diagram view (right). Strike-slip calculations shown in map view.

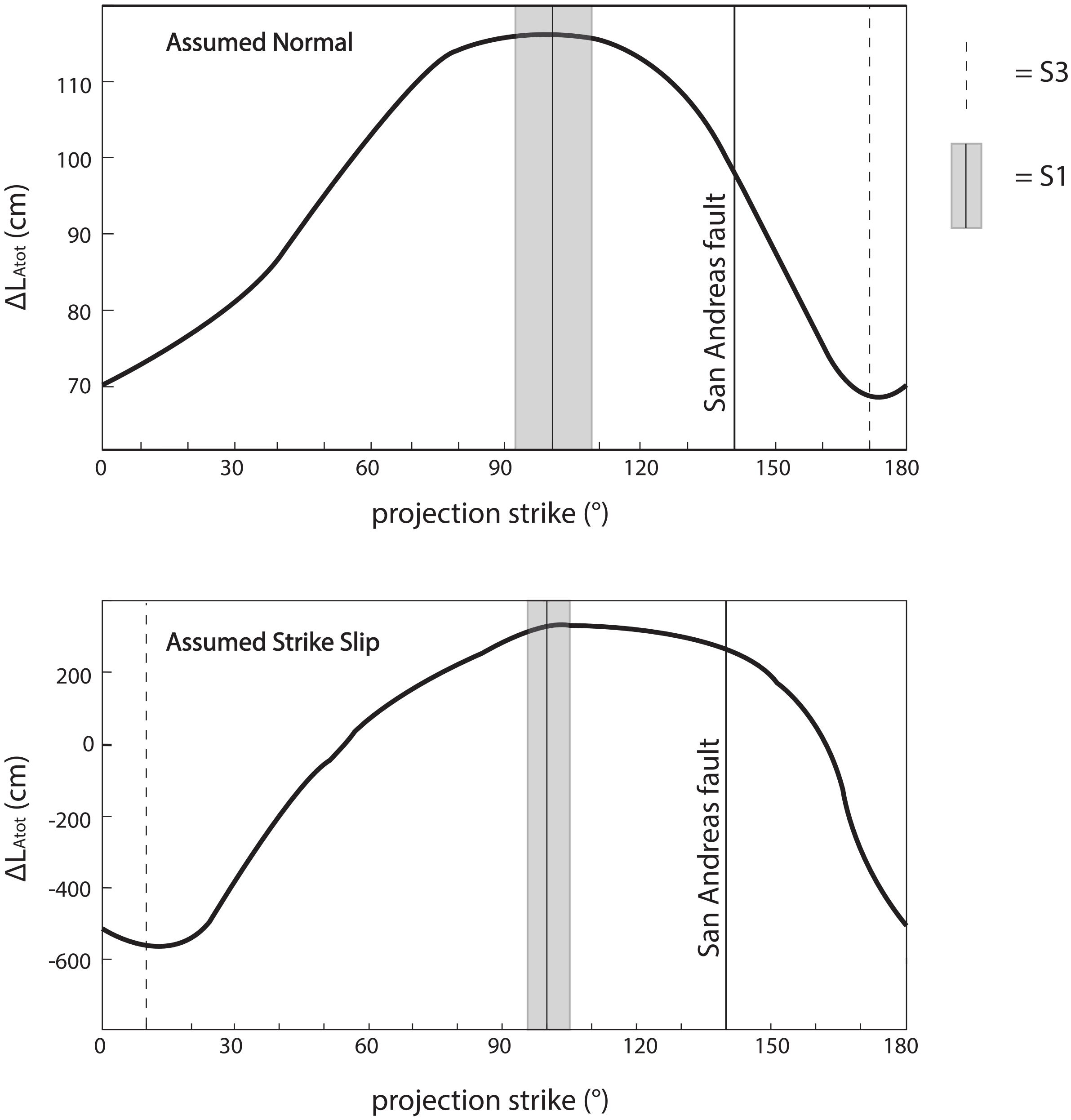

Figure 11. Graphs of total apparent change in length for projected transect orientions between 0-180°. Maximum ΔL_{Atot} corresponds with projection orientation parallel to the direction of maximum elongation (S1). Orientation with minimum ΔL_{Atot} is parallel to the direction of minimum elongation (S3). Results show S1 = 100° and S3 is between 350-010°.

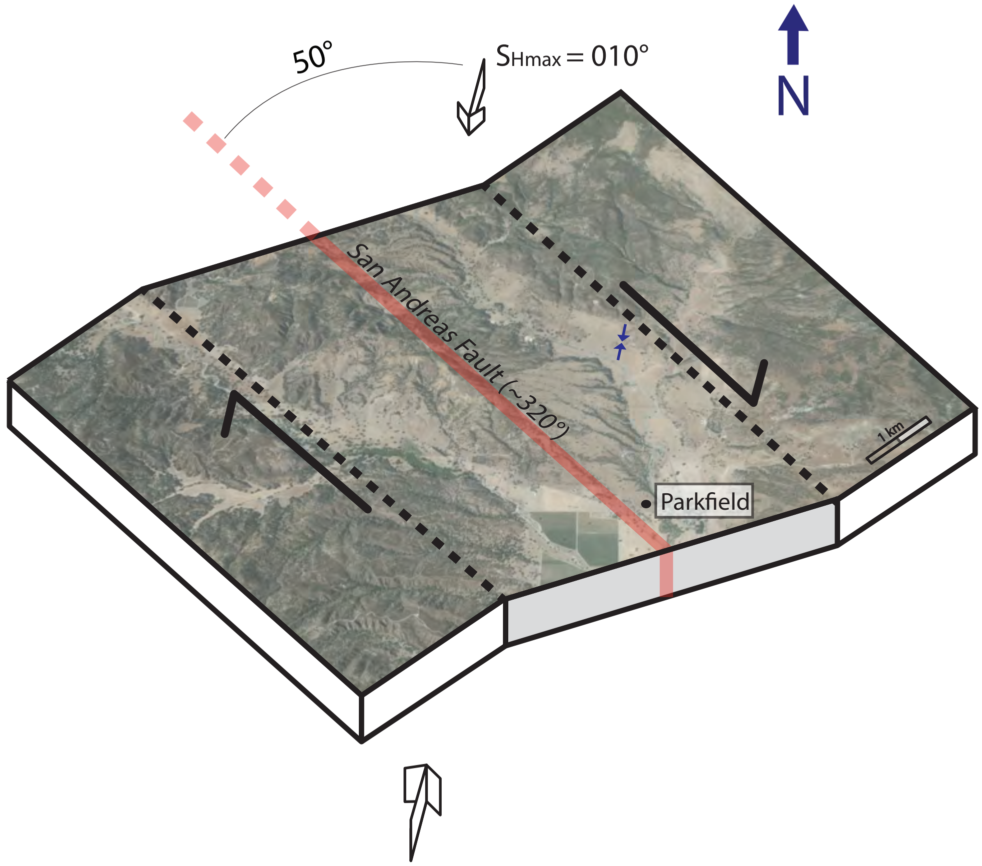

Figure 12. Wrench transpression hypothesis applied to the Parkfield region of the San Andreas fault. Study area marked by blue arrows, which align with the found S_{Hmax} value of 010°. Dotted lines show a minimum zone of mechanical weakness and distributed shear 2 km from the fault trace.

REFERENCES

Allmendinger, R.W., Siron, C.R., and Scott, C.P., 2017, Structural data collection with
mobile devices: Accuracy, redundancy, and best practices: Journal of Structural Geology, v. 102, p. 98-112

Bakun, W.H., and Lindh, A.G., 1985, The Parkfield, California, earthquake prediction experiment: Science, v. 229, p. 619-624

Bergh, S.G., Sylvester, A.G., Damte, A., and Indrevaer, K., 2019, Polyphase kinematic history of transpression along the Mecca Hills segment of the San Andreas fault, southern California: Geosphere, v. 15, p. 1-34

Byerlee, J.D., 1978, Friction of Rocks *in* Pure and Applied Geophysics, v. 116, p. 615-626

Cawood, A.J., et al., 2017, LiDAR, UAV, or compass-clinometer? Accuracy, coverage and the effects on structural models: Journal of Structural Geology, v. 98, p. 67-82

Dickinson, W.R., 1966, Structural relationships of San Andreas fault system, Cholame Valley, and Castle Mountain Range, California: Geological Society of America Bulletin, v. 77, p. 707-726

Dewez, T.J.B., Girardeau-Montaut, D., Allanic, C., and Rohmer, J.J., 2016, FACETS: A CloudCompare plugin to extract geological planes from unstructured 3D point clouds: The International Archives of the Photogrammetry, Remote Sensing and Spatial Information sciences, v. 41, p. 799-804

Fossen, H., Tikoff, B., and Teyssier, C., 1994, Strain modeling of transpressional and transtensional deformation: Norsk Geologisk Tidsskrift, v. 74, p. 134-145

Fossen, H., et al., 2007, Deformation bands in sandstone: a review: Journal of the Geological Society, London, v. 164, p. 755-769

Fossen, H., et al., 2017, A review of deformation bands in reservoir sandstones: geometris, mechanisms and distribution *in* Ashton, M., Dee, S.J., and Wennberg, O.P., eds., Subseismic-Scale Reservoir Deformation: Geological Society, London, Special Publications 459

Hardebeck, J.L., and Hauksson, E., 1999, Role of fluids in faulting inferred from stress field signatures: Science, v. 285, p. 236-239

Hardebeck, J.L., and Michael, A.J., 2004, Stress orientations at intermediate angles to the San Andreas Fault, California: Journal of Geophysical Research, v. 109, p. 1-16

Harding, T.P., 1976, Tectonic significance and hydrocarbon trapping consequences of sequential folding synchronous with San Andreas faulting, San Joaquin Valley, California: The American Association of Petroleum Geologists Bulletin, v. 60, p. 356-378

Lindquist, P., 2018, Deformation bands in the Etchegoin Formation sandstone: Triaxial deformation experiments and implications for principle stress directions in central California [Bachelor's thesis]: Carleton College, p. 1-57

Link, M.H., Helmold, K.P., and Long, W.T., Geologic description of upper Miocene Chanac and lower Pliocene Etchegoin formations: American Association of Petroleum Geologist Bulletin, v. 70

Loomis, K.B., 1990, Depositional environments and sedimentary history of the Etchegoin group, west-central San Joaquin Valley, California *in* Structure, Stratigraphy and Hydrocarbon Occurrences of the San Joaquin Basin, California, p. 231–246.

McEvilly, T.V., Bakun, W.H., and Casaday, K.B., 1967, The Parkfield, California, earthquakes of 1966: Bulletin of the Seismological Society of America, v. 57, p. 1221-1244

Mount, V.S., and Suppe, J., 1987, State of stress near the San Andreas fault: Implications for wrench tectonics: Geology, v. 15, p. 1143-1146

Newman, A.C., 2011, Using small-scale structures as a tool for understanding regional deformation: A study of deformation bands and faults at Kettleman Hills, California [Bachelor's thesis]: Carleton College, p.1-36.

Novakova, L., and Pavlis, T.L., 2017, Assessment of the precision of smart phones and tablets for measurement of planar orientations: A case study: Journal of Structural Geology, v. 97, p. 93-103

Scholz, C.H., Wyss, M., and Smith, S.W., 1969, Seismic and aseismic slip on the San Andreas fault: Journal of Geophysical Research, v. 74, p. 2049-2069

Schultz, R.A., and Siddharthan, R., 2005, A general framework for the occurrence and faulting of deformation bands in porous granular rocks: Tectonophysics, v. 411, p. 1-18

Smith, S.W., and Wyss, M., 1968, Displacement on the San Andreas fault subsequent to the 1966 Parkfield earthquake: Bulletin of the Seismological Society of America, v. 59, p. 1955-1973

Provost, A., and Houston, H., 2001, Orientation of the stress field surrounding the creeping section of the San Andreas fault: Evidence for a narrow mechanically weak fault zone: Journal of Geophysical Research, v. 106, p. 11373-11386

Tavani, S., et al., 2013, Building a virtual outrop, extracting geological information from it, and sharing the results in Google Earth via OpenPlot and Photoscan: An example from the Khaviz Anticline (Iran): Computers & Geoscience, v. 63, p. 44-53

Tavani, S., Corradetti, A., and Billi, A., 2016, High precision analysis of an embryonic extensional fault-related fold using 3D orthorectified virtual outcrops: the viewpoint importance in structural geology: Journal of Structural Geology, v. 86, p. 200-210

Scholz, C. H., 2000, Evidence for a strong San Andreas Fault: Geology (Boulder), v. 28, p. 163-166.

Sheirer, A.H., and Magoon, L.B., 2007, Age, distribution, and stratigraphic relationship of rock units in the San Joaquin Basin province, California, *in* Petroleum Systems and Geologic Assessment of Oil and Gas in the San Joaquin Basin Province, California: USGS Professional Paper 1713, ch. 5

Vasuki, Y., et al., 2014, Semi-automatic mapping of geological Structures using UAV-based photogrammetric data: An image analysis approach: Computers & Geosciences, v. 69, p. 22-32

Wentworth, C.M., and Zoback, M.D., 1989, The style of late Cenozoic deformation at the eastern front of the California coast ranges: Tectonics, v. 8, p. 237-246

Zoback, M.D., and Hickman, S., 2004, Stress orientations and magnitudes in the SAFOD pilot hole: Geophysical Research Letters, v. 31, p. 1-4

Zoback, M.D., et al., 1987, New evidence on the state of stress of the San Andreas fault system: Science, v. 238, p. 1105-1111
Zoback, M., Hickman, S., and Ellsworth, E., 2011, Scientific drilling into the San Andreas fault zone – An overview of SAFOD's first five years: Scientific Drilling, v. 11, p. 14-28

APPENDIX A

Example Excel code for calculating apparent change in length for a single deformation band assuming normal motion on a projected transect striking 180°.

Column key:
A = Dip direction azimuth (0-180°)
B = true change in length (ΔL_t)

Excel code:

```
=B2*(ABS(COS(RADIANS(ABS(A2-180)))))
```

APPENDIX B

Example Excel code for calculating apparent change in length for a single deformation band assuming strike-slip conditions on a projected transect striking 180°.

Rules:
If sense of motion is right lateral and the difference between the strike of the deformation band and the strike of the projection transect is greater than 90° OR between 0° and -90°, the observed change is negative (shortening).

If sense of motion is right lateral and the difference between the strike of the deformation band and the strike of the projection transect is less than 90° but greater than 0°, the observed change is positive (lengthening).

If sense of motion is left lateral and the difference between the strike of the deformation band and the strike of the projection transect is greater than 90° OR between 0° and -90°, the observed change is positive (lengthening).

If sense of motion is left lateral and the difference between the strike of the deformation band and the strike of the projection transect is less than 90° but greater than 0°, the observed change is negative (shortening).

Column key:
B = strike orientation of deformation band (0-180°)
D = assigned sense of motion (R = right lateral, L = left lateral)
E = n (# of deformation bands in cluster, n = 1 if single deformation band)

Excel code:

```
=IF(AND(D2="R", (B2-180)>90), E2*(ABS(COS(RADIANS(ABS(B2-180)))))*(-1),
IF(AND(D2="R", (B2-180)<90, (B2-180)>0), E2*(ABS(COS(RADIANS(ABS(B2-
180))))), IF(AND(D2="R", (B2-180)<0, (B2-180)>(-90)),
E2*(ABS(COS(RADIANS(ABS(B2-180)))))*(-1), IF(AND(D2="R", (B2-180)<(-90)),
E2*(ABS(COS(RADIANS(ABS(B2-180))))), IF(AND(D2="L", (B2-180)>90),
E2*(ABS(COS(RADIANS(ABS(B2-180))))), IF(AND(D2="L", (B2-180)<90, (B2-
180)>0), E2*(ABS(COS(RADIANS(ABS(B2-180)))))*(-1), IF(AND(D2="L", (B2-
180)<0, (B2-180)>(-90)), E2*(ABS(COS(RADIANS(ABS(B2-180))))),
IF(AND(D2="L", (B2-180)<(-90)), E2*(ABS(COS(RADIANS(ABS(B2-180)))))*(-
1)))))))))
```